Overview of LHD Experiments

M. Fujiwara, K. Kawahata, N. Ohyabu, O. Kaneko, A. Komori, H. Yamada, N. Ashikawa[1], L.R. Baylor[7], S.K. Combs[7], P.C. deVries, M. Emoto, A. Ejiri[3], P.W. Fisher[7], H. Funaba, M. Goto, D. Hartmann[8], K. Ida, H. Idei, S. Iio[4], K. Ikeda, S. Inagaki, N. Inoue, M. Isobe, S. Kado[3], K. Khlopenkov, T. Kobuchi[1], A.V. Krasilnikov[9], S. Kubo, R. Kumazawa, F. Leuterer[8], Y. Liang[1], J. F. Lyon[7], S. Masuzaki, T. Minami, J. Miyajima, T. Morisaki, S. Morita, S. Murakami, S. Muto T. Mutoh, Y. Nagayama, N. Nakajima, Y. Nakamura, H. Nakanishi, K. Narihara, K. Nishimura, N. Noda, T. Notake[2], S. Ohdachi, Y. Oka, S. Okajima[5], M. Okamoto, M. Osakabe, T. Ozaki, R.O. Pavlichenko, B.J. Peterson, A. Sagara, K. Saito[2], S. Sakakibara, R. Sakamoto, H. Sanuki, H. Sasao[1], M. Sasao, K. Sato, M. Sato, T. Seki, T. Shimozuma, M. Shoji, H. Sugama, H. Suzuki, M. Takechi, Y. Takeiri, N. Tamura, K. Tanaka, K. Toi, T. Tokuzawa, Y. Torii[2], K.Tsumori, K. Y. Watanabe, T. Watanabe, T. Wateri, I. Yamada, S. Yamaguchi, S. Yamamoto[2], M. Yokoyama, N. Yoshida[6], Y. Yoshimura, Y. P. Zhao[10], R. Akiyama, K. Haba, M. Iima, J. Kodaira, T. Takita, T. Tsuzuki, K. Yamauchi, H. Yonezu, H. Chikaraishi, S. Hamaguchi, S. Imagawa, N. Inoue, A. Iwamoto, S. Kitagawa, Y. Kubota, R. Maekawa, T. Mito, K. Murai, A. Nishimura, H. Chikaraishi, K. Takahata, H. Tamura, S. Yamada, N. Yanagi, K. Itoh, K. Matsuoka, K. Ohkubo, I. Ohtake, S. Satoh, T. Satow, S. Sudo, S. Tanahashi, K. Yamazaki, Y. Hamada, O. Motojima

National Institute for Fusion Science, Oroshi-cho 322-6, Toki 509-5292, Japan
[1] Graduate University for Advanced Studies, Hayama 240-0193, Japan
[2] Dep. of Energy Eng. and Science, Nagoya University, Nagoya 464-8603, Japan
[3] University of Tokyo, Tokyo 113, Japan
[4] Tokyo Institute of Technology, Meguro-ku, Tokyo 152-8550, Japan
[5] Chubu University, Kasugai-shi 487-8501, Japan
[6] Kyushu University, Kasuga-shi 816-8580, Japan
[7] Oak Ridge National Laboratory, Oak Ridge, Tennessee, 37831-8072 USA
[8] Max Plank Institute for Plasma Physics, D-85748, Garching, Germany
[9] Troitsk Institute of Nuclear Physics (TRINITI), Troitsk, Russia
[10] Institute of Plasma Physics, Academia Scinica, 230031, Hefei, Anhui, China

e-mail contact main author: Fujiwara@nifs.ac.jp

Abstract. Experimental studies on the Large Helical Device during the last two years are reviewed. After the start of LHD experiment in 1998, the magnetic field has been gradually raised up to 2.89 T. The heating power has been increased, up to 4.2 MW for NBI, 1.3 MW for ICRF, and 0.9 MW for ECRH. Upgrading the key hardware systems has led to the extension of the plasma parameters to (i) higher T_e [$T_e(0)$ = 4.4 keV at <ne> = 5.3 x 10^{18} m^{-3} and P_{abs} = 1.8 MW], (ii) higher confinement [τ_E = 0.3 s, $T_e(0)$ = 1.1 keV at $<n_e>$ = 6.5 x 10^{19} m^{-3} and P_{abs} = 2.0 MW] and (iii) higher stored energy W_p^{dia} = 880 kJ. High performance plasmas have been realized in the inward shifted magnetic axis configuration (R=3.6m) where the helical symmetry is recovered and the particle orbit properties are improved by trade off of MHD stability properties due to the appearance of the magnetic hill. The energy confinement was systematically higher than that predicted by the International Stellerator Scaling 95 up to a factor of 1.6 and was comparable with ELMy H-mode confinement capability in tokamaks. This confinement improvement is attributed to the configuration control (the inward shift of magnetic axis) and to the formation of the high edge temperature. The achieved average beta value reached 2.4 % at B=1.3 T, the highest beta value ever obtained in helical devices, and so far no degradation of confinement by MHD phenomenon is observed. The inward shifted configuration has also led to successful ICRF minority ion heating. ICRF power up to 1.3 MW was reliably injected into the plasma without significant impurity contamination and a plasma with a stored energy of 200 kJ was sustained for 5 sec by ICRF alone. As another important result long pulse discharges of more than 1 minute were successfully achieved separately with NBI heating of 0.5 MW and with ICRF heating of 0.85 MW.

1. Introduction

The Large Helical Device (LHD) [1-4] is the world's largest heliotron type device with l=2/m=10 continuous helical coils and three pairs of poloidal coils. The major and minor radii of the plasma are 3.6 - 3.9 m and 0.6 - 0.65 m, respectively. The main objective of the LHD program is to develop physics and technologies for a steady state fusion reactor in which a fusion plasma is confined in externally given magnetic fields and the recircurating power is expected quite low. The results obtained so far in small or medium sized helical devices seemed feasible, however, realized parameters are still far from those of fusion reactor. The main role of LHD is to extend the parameter regimes and to demonstrate the feasibility of helical type fusion reactor by realizing the confinement of higher temperature, fusion relevant plasmas in long pulse/steady state condition. The choice of l=2/m=10 configuration is the result of the optimization for the MHD limit and confinement properties and the employment of the continuous winding is for keeping clean helical divertor structures to make diverted helical plasmas. Utilizing superconducting helical and poloidal field coils, it is possible to investigate current-less and disruption-free steady-state plasmas in a reactor-relevant plasma regime. In the first experimental campaign (Mar. to May 1998)[3,4], plasma was generated and heated by ECH alone by using two gyrotron tubes (84 and 82.6 GHz). The basic performance of LHD is confirmed in this experiment: (1) the high accuracy of LHD magnetic fields confirmed by magnetic flux mapping using the fluorescence method, (2) high temperature plasmas of more than 1 keV and (3) energy confinement time of more than 0.2s.

In the 2nd experimental campaign (Sept. to Dec. 1998), neutral beam injection (NBI) heating started by using two tangential beam lines (co- and counter-injection). A comprehensive set of diagnostic instruments was installed before the start of the 2nd campaign as is shown in Fig.1. The spatial and temporal behaviors of the electron density ne(r,t), the electron temperature Te(r,t) and the ion temperature Ti(r,t) are measured with a 13-channel FIR laser interferometer [5], a 120-channel YAG Thomson scattering [6] and charge exchange recombination spectroscopy (CXRS), respectively. A pair of ICRF antennas was installed from the top and the bottom vertical ports of LHD. The magnetic field strength was 1.5 T, the same as that used in the first campaign, and increased up to 2.75 T successfully at the end

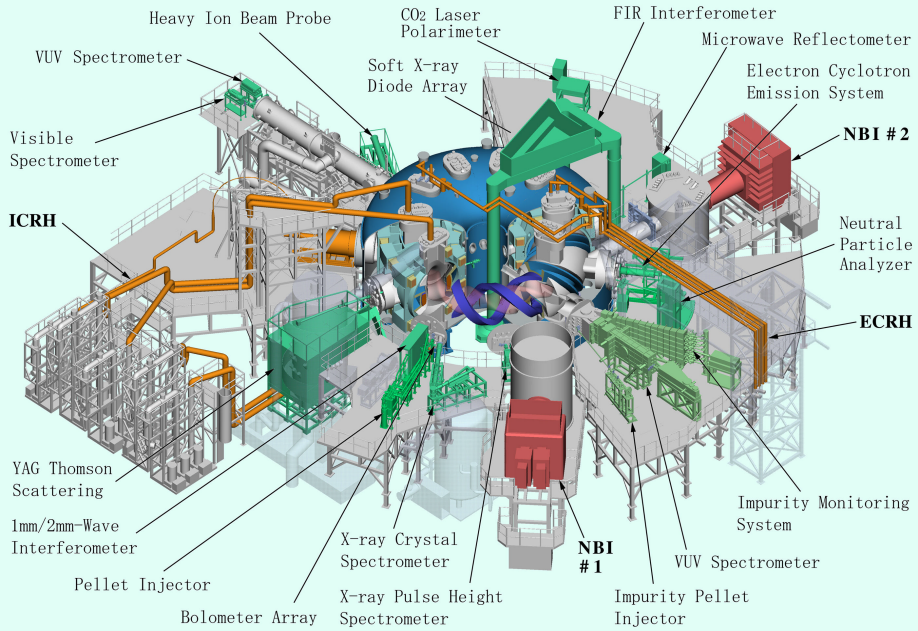

Fig. 1 Location of LHD diagnostic systems and heating systems.

of the 2nd experimental campaign.

In the 3rd experimental campaign (Jul. to Dec. 1999), the magnetic field was gradually increased while checking carefully the stability of the SC conductors, and the maximum magnetic field was 2.89 T at the magnetic axis of R_{ax} = 3.6 m. The heating power has been gradually increased, i.e., NBI up to 4.2 MW (with two beam lines), ICRF up to 1.3MW (with one antenna system), and ECRH up to 0.9 MW (with six gyrotron tubes). The specifications of each heating source are summarized in Table 1 including LHD machine parameters. Carbon tiles were installed as divertor plates to meet high power heatings, resulting in significant reduction in metal impurity concentration (Fe) and total radiation power. As a new instrument for controlling particle fueling, a multi-pellet injector was developed and routinely applied. The pellet injector has five independent barrels, and the size and velocity of each pellet are 3 mmϕ x 3 mm*l* and 1 km/s, respectively. The pellet injection has extended the operational density regime of NBI plasmas up to 1.1 x 10^{20} m^{-3}, which is 2 times higher than that estimated from the empirical scaling of the density limit in helical devices [7], and contributes to achievement of high beta plasmas.

Table 1. Specifications of LHD and Heating Systems

Major radius R	3.6 – 3.9 m
Minor radius a	0.6 – 0.65 m
Plasma volume V_p	20 – 30 m^3
l, m	2, 10
Coil minor radius a_c	0.975 m
Magnetic field B_t	3 (4) T
Magnetic energy	0.9 (1.6) GJ
Heating power	
NBI (15 MW)	2 beam lines 180 keV, H-beam 7.5 MW/beam line
ECH (10 MW)	84 GHz 168 GHz
ICRH (12 MW)	25 - 95 MHz 12 MW – pulse 3 MW – steady state

2. Confinement Properties

One of the unique features of LHD plasmas is the formation of the edge pedestal without a rapid transition that is usually observed in the H-mode discharges on other machines. The energy confinement was systematically better than that predicted by the International Stellerator Scaling 95 [8] up to a factor of 1.6. The temperature pedestal observed contributes to this enhancement. Figure 2 shows the temporal evolution of a typical NBI heated plasma with the injection power of 3.1 MW. When neutral beams are injected into a target plasma generated by ECH, the hot plasma region expands radially and eventually reaches the last closed magnetic flux surface and finally reaches the divertor plates. During this build up phase, the temperature pedestal [9] is formed without a rapid transition. In the figure the stored energy (W_p), electron density (n_e), and radiation power (P_{rad}) keep steady state levels after the gas puffing is turned off. The global energy confinement time, defined by $\tau_E = W_p/P_{abs}$, is about 250 ms, which is longer than the τ_E (ISS95) by the factor of 1.5, where τ_E (ISS95) is the energy confinement time predicted by the international stellarator scaling ISS95.

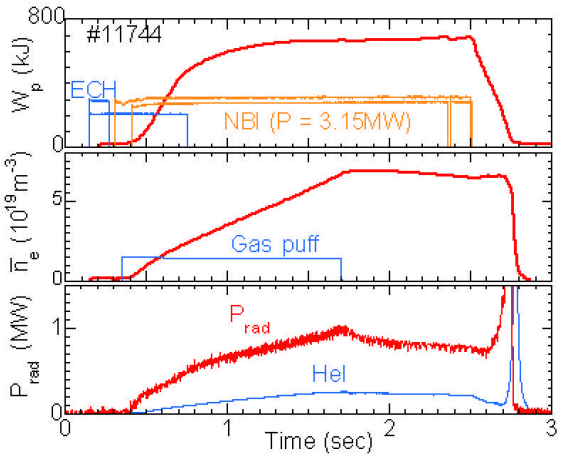

Fig. 2 Temporal evolution of a typical LHD plasma discharge. W_p is the total stored energy and P_{rad} is the total radiation power measured by a bolometric system

Figure 3 shows electron temperature profiles from discharges with two somewhat extreme plasma parameters as follows; (a) one of the highest store energy plasmas, W_p = 760 kJ, n_e

= 6.3 x 10^{19} m^{-3} , B = 2.75 T, (b) one of high beta plasmas, <β> = 1.3 %, n_e = 2.3 x 10^{19} m^{-3}, B = 0.75 T. The shape of the T_e profile, however, is similar with a very broad profile, and often shows a bend (temperature pedestal [9]) in the slope of the profile at ρ ~ 0.85 especially in helium discharges. One of the remarkable features of the LHD discharges is the high edge temperature T_e^{edge} (T_e at ρ = 0.85), which is found to be (0.3 – 0.5) x $T_e(0)$. Thus W_p is almost proportional to $n_e T_e^{edge}$ and thus τ_E is predominantly determined by the edge confinement. A similar improvement in edge confinement has been observed in smaller helical devices [10,11] when the last closed magnetic flux surface is close to the magnetic rational surfaces. In the LHD configuration, the $i/2\pi$ = 1 surface is always located in the edge region where the pedestal exists. Hence the $i/2\pi$ = 1 surface or its associated island (m/n = 1/1) could play some role in the formation of the high edge temperature in LHD.

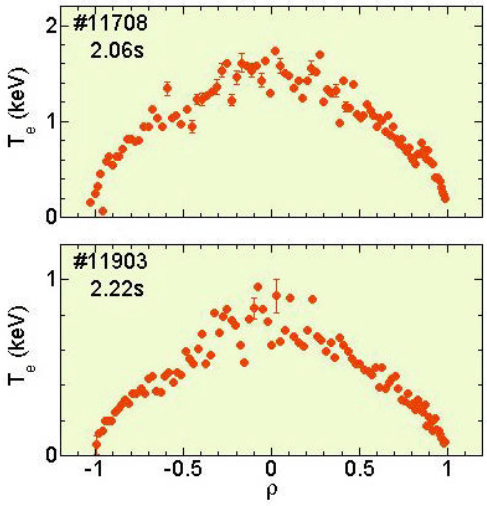

Fig. 3 Temperature profiles of helium plasmas for a high plasma pressure discharge (a) and for a high beta discharge (b).

The database on global energy confinement compiled during the last two years is compared with the International Stellarator Scaling 95 shown in Fig. 4. It comprises of a total of 177 NBI heated discharges with hydrogen plasma. The parameter regime included here covers a magnetic field strength of 0.75 - 2.9 T, a line averaged electron density of 1.0 – 7.0 x 10^{19} m^{-3}, and heating power of 0.5 - 4.2 MW. The discharge with the inward shifted configuration (R_{ax} = 3.6 m) exhibits a factor of 1.6 improvement over the ISS95 scaling and the confinement is comparable to those of ELMy H-mode tokamaks.

Neoclassical theory suggests that helical ripple transport can be mitigated by a multi-helicity effect in the inward shifted configuration. An anomalous transport model based on the self-sustained turbulence due to interchange modes also suggests that the heat conduction coefficient could be improved by 20-30% by strong magnetic shear in the peripheral region in the case of the inward shifted configuration [12].

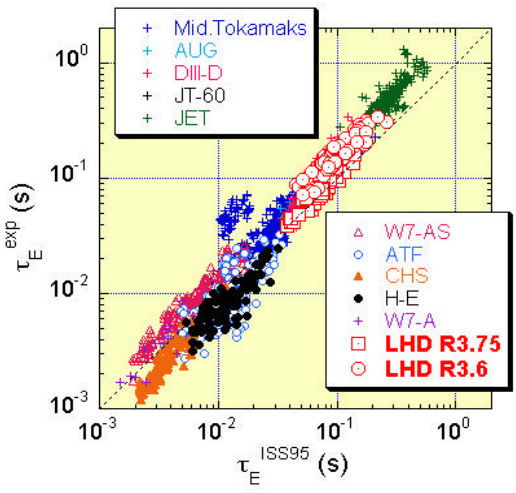

Fig 4 Comparison between experimental values of energy confinement and those predicted from ISS95 scaling. (tokamak data from ITER H-mode Database, Ver.5)

Figure 5 shows the temperature and density profiles and the analyzed heat conduction coefficient in dimensionally similar plasmas with different magnetic axes. The temperature is adjusted by controlling the heating power for the same line averaged density. A 60 % larger heating power is required for the standard configuration (R_{ax} = 3.75 m) to get the same temperature as in the inward shifted configuration. Hollowness in the density profile is enhanced in the standard configuration which suggests the neoclassical off-diagonal particle diffusion due to the temperature gradient. The predominant heat loss channel is electron

conduction since the 80 % of the NBI power is deposited to electrons in the present condition. Electron heat diffusivity decreases in the inward shifted configuration, which is consistent with the characteristics of the energy confinement time. The improvement in the intermediate region ($\rho \sim 0.5$) could be due to the reduction of neoclassical heat flux if the experimental observation is a simple sum of the anomalous transport common to both cases and the neoclassical transport. The contribution of the neoclassical transport is 50 % in the standard case while it decreases to one forth in the inward shifted case. Anomaly in the peripheral region becomes more than twice that in the intermediate region. The inward shifted case still shows improvement in the peripheral region as well although the neoclassical transport does not explain this feature.

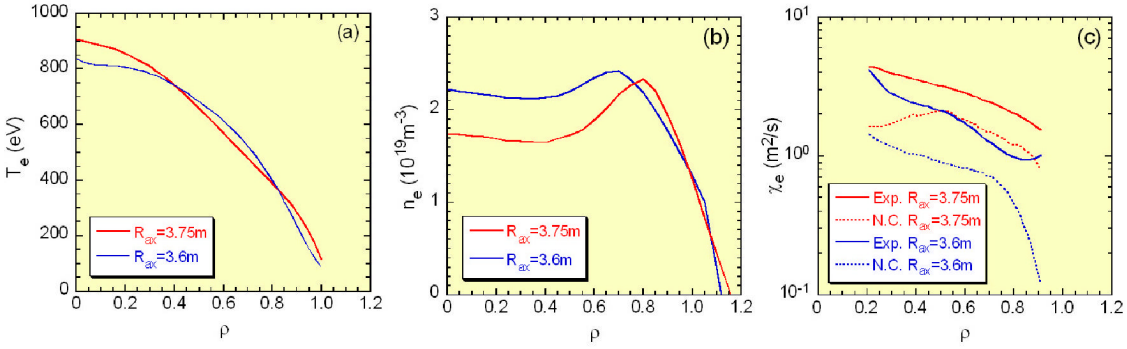

Fig. 5 Spatial profiles of electron temperature (a), density (b), and the analyzed heat conduction coefficient (c) in dimensionally similar hydrogen plasmas with different magnetic axes.

For precise experimental data analysis and simulation on LHD, a 3-dimensional equilibrium / 1-dimensional transport code TOTAL (Toroidal Transport Analysis Linkage) [13] with the PRE-TOTAL code for experimental data interface has been developed as an extension of previous HSTR code [14]. This code is characterized by the inclusion of the self-consistent equilibrium with experimental data, magnetic multiple-helicity effect and radial electric field effects on neoclassical transport, time-varying NBI deposition profile, and bootstrap current effects on equilibrium-transport. For the experimental data analysis of local transport, the self-consistent equilibrium has been treated in the TOTAL code and PRE-TOTAL code with measured radial profiles by 13-channel FIR laser density measurement and 120-channel YAG Thomson scattering electron temperature measurement. Ion density and temperature profiles are assumed to be equal to those of electrons, which is confirmed in some typical medium discharges. The NBI power deposition is calculated by the TOTAL code, and the effective thermal diffusivity χ_{eff} is defined as $\chi_{eff} = - (Q_{NBI} + Q_{RF} - dW/dt)/(2.5ndT/dr)$, assuming $T_i \sim T_e$. To clarify the relationship between global and local transport, we used the same experimental database to evaluate both the global and local transport based on kinetic pressure instead of diamagnetic energy [15]. The ion temperature was not routinely measured and we assumed the same temperature profile as the electron temperature. The global kinetic pressure obtained using this assumption is consistent with slightly the diamagnetic energy obtained by the magnetic measurement with the accuracy of 10 %. Here it should be noted that MHD equilibria are calculated iteratively and self-consistently.

Dimensionless analysis based on Kadomtsev's constraints [16] is used in the log-linear regression analysis of experimental data. Here, we adopted a special method to add dimensional constraints. For the radial profile analysis, we use the following dimensionally normalized formulas: $\chi_E/(B_r^2) \sim 10^c \rho_*^{c_\rho} \nu_{0*}^{c_\nu} \beta^{c_\beta}$. The exponents of each parameter are obtained as a function of normalized minor radius by regression analysis as shown in Fig.6. It is found that the radial distribution lies between gyro-Bohm and Bohm in the core and strong

gyro-Bohm in the boundary. The transport properties are suggested to be changed near the boundary.

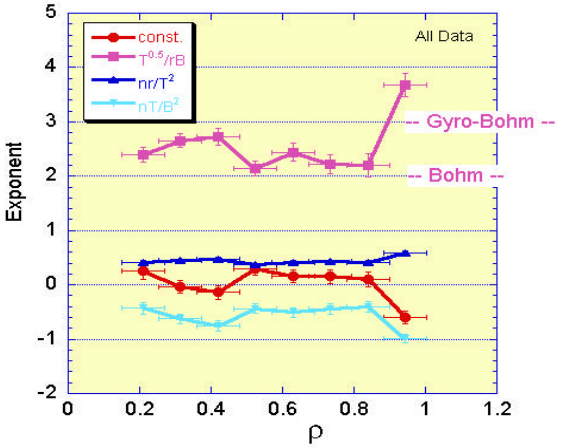

Fig. 6 Exponents of dimensionless $c_E / (Br^2)$ scaling vs. normalized minor radius

In helical systems, the radial electric field is one of the key parameters for confinement of a high temperature plasma because neoclassical theory suggests that an electric field reduces the helical ripple loss and consequently improve the energy confinement. Er-bifurcation property predicted by neoclassical theory is confirmed in CHS, and the property is the cause of the electron thermal transport barrier formation [17].

Figure 7(a) shows the density dependence of the radial electric field near the plasma edge (ρ = 0.9) for the plasma heated by NBI. The magnetic field strength is 0.75. 1.5 and 2.5 T at the magnetic axis of R_{ax} = 3.75 m. The central ion temperature is 0.6 keV (at 0.75 T) to 2.0 keV (at 2.5 T) and close to the central electron temperature. The radial electric field is derived from the poloidal and toroidal rotation velocity and pressure gradient of the Neon impurity with charge exchange recombination spectroscopy using the radial force balance. The observed electric field is negative (ion root), around 5 keV in the electron density range of 1.0 – 3.0 x 10^{19} m^{-3}. On the other hand, the transition from ion root (negative radial electric field) to electron root (positive electric field) is observed in the low density regime below 1 x 10^{19} m^{-3}. The edge radial electric field increased up to 15kV/m in the electron root as the density was decreased to 0.4 x 10^{19} m^{-3}. The transition from ion root to electron root was observed at ρ > 0.8 and the radial electric field is very low in the plasma core (see Fig. 7(b)). The measured electric field is compared with that predicted by neoclassical theory, and qualitative agreement with them is obtained as is also shown in Fig.7.

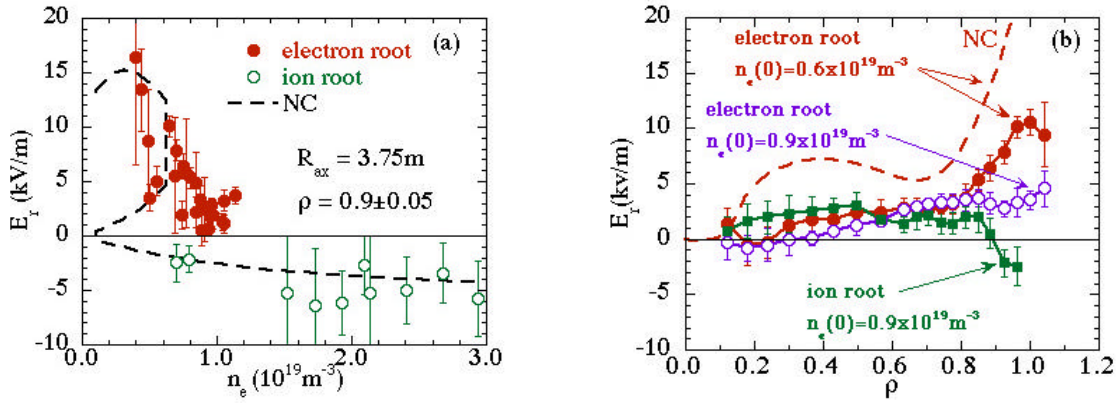

Fig. 7 (a) Density dependence of radial electric field near edge (r = 0.9) and (b) radial profiles of radial electric field in the density region at the transition from ion root to electron root for the plasmas heated by NBI.

3. ICRF Heating and Energetic Particle Confinement

The first trial of the ion cyclotron range of frequencies (ICRF) heating in LHD was carried out [18] in helium plasma with minority hydrogen ions during the second experimental campaign of 1998. In this experiment, the magnetic field strength was fixed at 1.5 T with an RF frequency of 25.6 MHz and the major radius of the magnetic axis was also fixed at 3.75 m. The target plasma was produced by the 2nd harmonic ECH of 84 GHz and a low electron

density of less than 1.0 x 10^{19} m^{-3}. Consequently the low coupling resistance (~ one ohm) limited the maximum injection power to less than 300 kW. The maximum increase in the stored energy was 3 kJ at P_{ICH} = 300 kW. In this series of the experiment, we chose the heating mode to be the electron heating mode since minority ion heating was thought to encounter difficult impurity problems caused by the production of high energy ions.

In the 3rd experimental campaign, drastically improved heating performance was achieved with the ion heating mode. The most efficient heating was obtained in the case where the resonance layer of minority ions was located near the saddle point of the mod-B profiles. The injected RF power was mostly absorbed by minority ions. ICRF power up to 1.3 MW was reliably injected into the plasma and a 200 kJ plasma was sustained for 5 sec by ICRF alone without significant increase in impurity concentration [19]. The best parameters of the plasma sustained by ICRF alone are: W_p ~ 200 kJ, n_e ~ 1.8 x 10^{19} m^{-3} and Te ~ Ti ~ 2 keV. This high heating performance was achieved by upgrading the machine from the 2nd campaign as follows: (i) an increase in the magnetic field strength, usually 2.75 T, (ii) improvement of particle orbit due to inward shift of the magnetic axis (R_{ax} = 3.6 m) and (iii) reduction of iron impurities by means of adoption of graphite divertor plates. Figure 8 shows the time evolution of the plasma sustained by ICRF alone (a) compared with that of the plasma sustained by NBI alone (b). In order to compare properties of each heating scheme easily, both the target plasma density and absorbed power by the plasma were set at almost the same values. Here, the absorbed power can be estimated by the decay of the plasma-stored energy for ICRF heating and by the measurement of shine-through power in the case of NBI heating. The absorbed power at the density of 1.0 x 10^{19} m^{-3} was about 1 MW in both cases. The parameters of ICRF

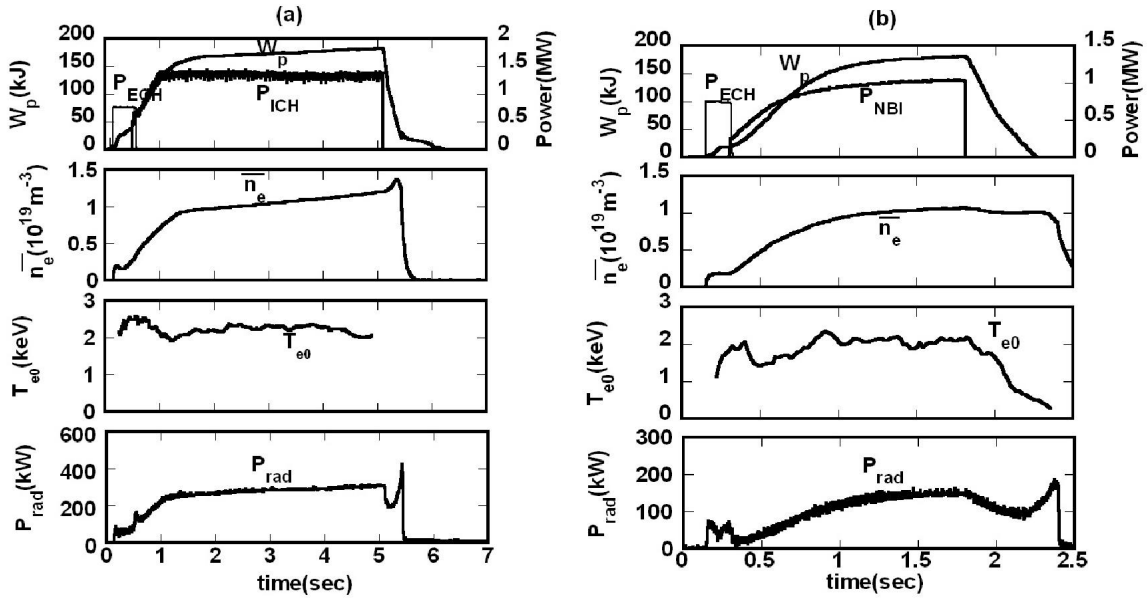

Fig. 8 Time evolution of the plasmas sustained by ICRF alone (a) and by NBI alone (b).

sustained plasma were similar to those of the NBI sustained plasma. The stored energy and the central electron temperature were ~170 kJ and 2.2 keV, respectively. The heating efficiency of the ICRF heating was similar to that of NBI heating. This means that high-energy trapped particles are well confined in the LHD helical magnetic field as well as the high-energy passing particles. In order to see the confinement of high-energy particles more directly, the high-energy tail component was measured using a Natural Diamond Detector [20]. Figure 9 shows the energy spectrum of the hydrogen ions before and after RF switch on. It is noted that high-energy tail extends to 200 keV indicating that high energy ions are well confined.

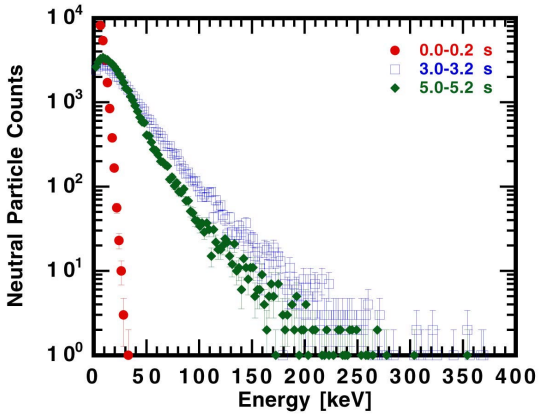

Fig. 9 Perpendicular particle spectra of high energy ions generated by ICRF heating.

4. High Beta Plasmas and MHD Stability

In NBI discharges in LHD, the plasma can be started up [21] by NBI alone. This technique is unique to helical systems that have a vacuum magnetic field configuration which confines high energy ions. It is useful for the experiment because the magnetic field strength can be changed without any experimental constraint on the magnetic field required by ECH. We have already reported on plasma start up by NBI alone in Ref.[21], where the mechanism of plasma buildup by neutral beams alone was described. The main process is the ionization of the background neutrals by the ionized beam component, which is estimated to be about 2% of the injection beam. The key point to build up the plasma is to keep the beam injection into a very thin plasma of less than 1 x 10^{18} m^{-3} without gas puffing for several hundreds of milliseconds. The confined fast ions ionize the background neutrals and heat up the electrons. After the plasma electron is heated sufficiently to ionize background neutrals, a proper amount of gas puffing is applied to build up the plasma density. In the 3rd experimental campaign, by using this technique the dependence of the confinement on a wide range of the magnetic field strength (0.5 – 2.89 T) is studied and high β plasmas are achieved at the low magnetic field. The obtained maximum average β value is 2.4 % at B=1.3 T with the help of pellet injection, which is the highest β value ever obtained in helical devices [22, 23].

Figure 10 shows a temporal evolution of a typical high β plasma achieved by using the new plasma initiation technique described above. The magnetic field strength is 0.75 T at the magnetic axis of R_{ax} = 3.6 m. The target plasma is initiated and sustained by using two neutral beam lines. The absorbed beam power was evaluated from the measurement of the shine-through power using a calorimeter array [24] installed on the armor tiles of the NBI. The volume averaged beta measured by a diamagnetic loop increases with the density, and reaches 2.1 % and is sustained during 1.4 s. The line-averaged electron density $\langle n_e \rangle$ and the central electron temperature $T_e(0)$ are about 3 x 10^{19} m^{-3} and 1 keV, respectively. The kinetic beta value estimated using these values are also plotted in Fig. 10, and are found to be consistent with the diamagnetic beta. The global energy confinement time is about 50 ms at the maximum beta value, which is about 1.2 times τ_E(ISS95). The magnetic fluctuations measured by Mirnov coils show that the total power (f = 0.1 – 50 kHz) of the magnetic fluctuation increases with the plasma beta value at first, and seems to be saturated in the high beta range of β > 1 %. The observed saturation level is quite low ($\tilde{b}/B < 10^{-4}$). The dominant modes observed in the high β region are m/n = 1/1 and its harmonics, which are considered to be the resistive interchange mode localized near the $\iota/2\pi = 1$ surface.

Figure 11 shows the Mercier stability diagram [25] in the LHD configuration. In the case of the standard magnetic field configuration (R_{ax} = 3.75 m) on LHD, the unstable region is localized in the peripheral region of the plasma. On the other hand, the plasma confined in inward shifted configuration (R_{ax} = 3.6 m) is unstable against the interchange mode in almost the whole region of the plasma, because the inward shifted configuration is a magnetic hill configuration. In the experiments, however, we observed no gross MHD phenomena which influence the plasma transport even in the plasma beta range up to 2.4 % though their appearance seems to be consistent with linear analyses of the interchange modes. More detailed analysis of the magnetic fluctuations is reported in a separate paper [26].

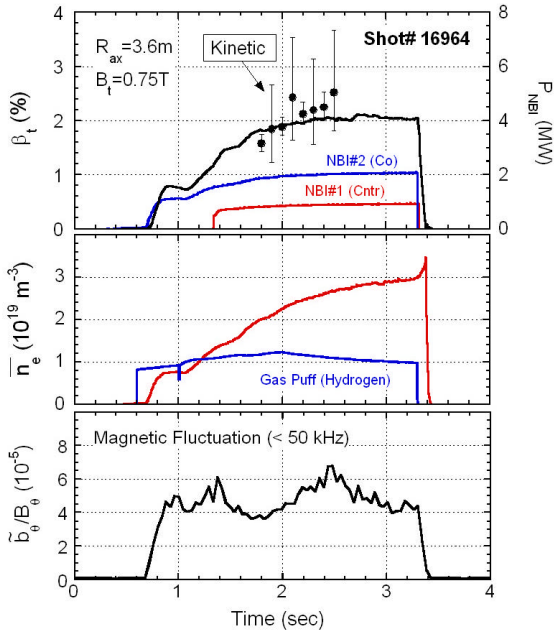

Fig. 10 Time trace of volume averaged beta, line-averaged electron density and a total power of the magnetic fluctuation in the frequency range of 0.1 – 50 kHz.

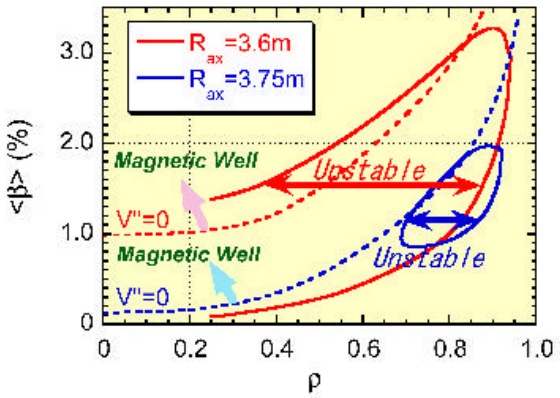

Fig. 11 Contour map of normalized Mercier stability criterion DI = 0 obtained by VMEC equilibrium calculation for the configurations of R_{ax} = 3.75 m and 3.6 m.

5. Long Pulse Operations

One of the main objectives of the LHD experimental program is to demonstrate current-less and disruption-free steady state plasmas with high performance of confinement. The goal of the steady-state operation in the early stage of LHD is to demonstrate a one hour discharge with 3 MW heating power [27]. In order to realize this goal, the plasma vacuum vessel and divertor plates are actively cooled by water, and a heat load of 3 MW can be removed continuously. Heating systems (ECH, NBI and ICRH) are also designed for long pulse operation. The near term goals of each heating system are as follows: (1) 1 MW/cw operation of ECH by using two gyrotrons of 84 GHz [28]; (2) 1 MW/30 min. operation of NBI [29]; (3) 3 MW/1 hour operation of ICRH [30].

The first long pulse experiment with NBI was carried out in the 2nd experimental campaign in 1998 [31]. By injecting 0.7 MW of NBI a plasma with the density of 0.3 x 10^{19} m^{-3} was sustained for 22 s. The available density regime with long pulse discharges, however, was limited to less than of 0.3 x 10^{19} m^{-3} by relaxation oscillation phenomena [31]. In this oscillating plasma “breathing plasma”, the TV image of the plasma shows that expansion and contraction of the hot core plasma repeated with a period of 1-2 s. Figure 12 shows an example of the breathing plasma that lasted for 20 s. The magnetic field strength is 1.5 T at the magnetic axis of 3.75 m. The injection energy and power of NBI are 66 keV and 0.6 MW, respectively. The gas puffing is applied only in the ECH plasma phase. The sawtooth-like density oscillation observed is considered to be closely related with the electron temperature in an ergodic region between the last closed magnetic flux surfaces (LCMS) and the separatrix. That is, the penetration rate of neutral particles into the core plasma depends on the electron temperature of the plasma confined between the LCMS and the separatrix. The rising phase of the density corresponds to the expansion phase of the plasma. During this phase, the plasma continues to expand radially with NBI heating and reaches the LCMS and divertor plates leading to a sudden increase of the ion saturation current of the Langmuir probe installed in the divertor. Similar phenomena are also observed in density clamping [32].

Periodic oscillation of the ion saturation current implies that this phenomenon is closely related to a repetition of the plasma detachment and reattachment to the divertor plates. Strong interaction between the plasma and the divertor plates in the reattachment phase causes an increase of ion impurity influx resulting in a decrease of electron temperature of the core plasma. Consequently, the heat flow to the plasma edge region decreases, leading to shrinking and detachment of the plasma. As a result, iron impurity influx decreases and then the core temperature increases again. More intensive discussions of this breathing plasma are given in Ref. [33]. After the installation of graphite tiles on the divertor traces between the 2nd and the 3rd experimental campaigns, we have no observation of breathing plasmas except in the case of the more inward shifted operation of the magnetic axis (R_{ax} = 3.5 m). In this magnetic configuration, the plasma contacts with the inboard wall (stainless steel) of the vacuum vessel (limiter discharge).

Long pulse discharges of more than one minute were successfully achieved with NBI heating (0.5MW) alone and with ICRF heating (0.85 MW) alone. Figure 13 shows the time evolution of the longest discharge sustained by NBI injection. The neutral beam is successfully injected for 80 sec with an injection power of 100 keV-0.5 MW. The magnetic field strength is 2.75 T at the magnetic axis of 3.6 m. The line–averaged density is kept constant (1.3 x 10^{19} m^{-3}) by a gas puff system with a feedback loop for the first 15 sec, and subsequently controlled manually by watching the colour of the plasma light on the TV monitor. The density oscillation with a long period of 40 sec is caused by the manual control of the helium gas puffing not by other uncontrollable effects. The central ion temperature, measured by Doppler broadening of TiXXI, is kept constant around 1.5 keV until the end of the discharge, and radiation power is nearly constant at a radiated power fraction of ~30 % as well as the impurity emission line intensities. The wall pumping of helium gas continues up to the end of the discharge, therefore the density can be controlled by the gas puffing. In this discharge the plasma current is observed to be 38 kA at the maximum. There are two kinds of toroidal

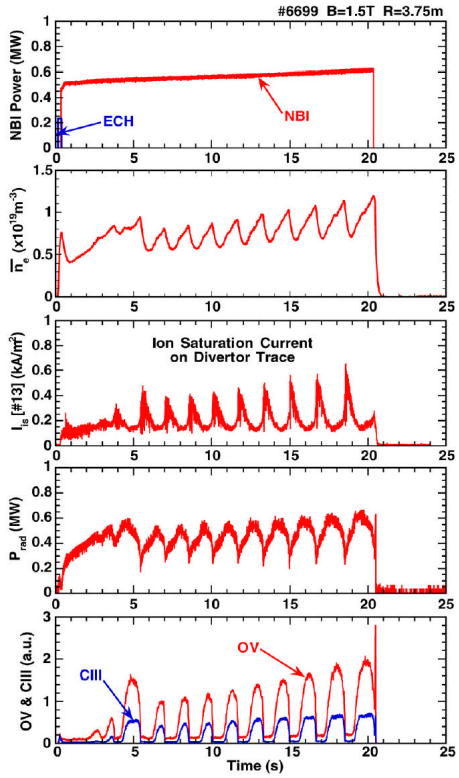

Fig. 12 Relaxation oscillation in an NBI discharge with a relatively high density at B = 1.5 T.

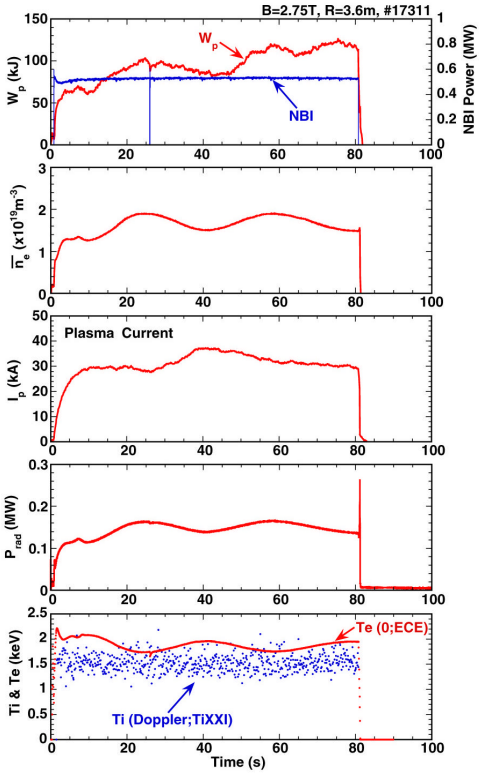

Fig. 13 Time evolution of plasma parameters of the longest pulse discharge sustained by NBI

current, bootstrap current and Ohkawa current. The bootstrap current estimated from the plasma pressure profile is about 5 kA and hence the Ohkawa current is the main component. With balanced beam injection the Ohkawa current can be canceled out. The highest bootstrap current is observed to be about 50 kA in high power heating experiments. So far we observe no clear effect on the confinement of the plasma by the toroidal current, which should be one of the issues in near future experiments with powerful heating.

6. Summary

The recent results of LHD experiments are reviewed focusing on key issues for fusion-relevant high temperature plasmas confined in non axi-symmetric toroidal magnetic configurations, which have an intrinsic advantage for steady state operation with low circulating power due to the existence of the vacuum magnetic surface. Issues to be studied are mainly related to the non symmetric configuration. The LHD was originally designed with l/m=2/10 and the aspect ratio A=6~7 and is optimized from various points of view such as MHD stability by the magnetic well due to toroidicity, the particle orbit/confinement by keeping a permissible degree of helical symmetry, the formation of clean helical divertor structure using continuous helical windings, the use of superconducting coils for steady state operation and so on. The main target of LHD experiments is to demonstrate the good confinement capability of higher beta plasmas in long pulse/steady state operation. The LHD experiment has made great progress in this direction as is summarized in the following.

1. MHD stable plasmas are obtained in the range of $<\beta> \sim 2.4\%$ in the inward shifted magnetic axis configuration which is considered to be unstable for Mercier criterion. These results are very similar with those of previous CHS experiments. The observed magnetic fluctuation level is quite low around 10^{-4} and has no effect on plasma confinement. The achievable critical beta is very important for the inward shifted configuration which is good for plasma and energetic particle confinement.

2. The confinement capabilities are measured by the comparison with the conventional stellarator scaling ISS95 and the global energy confinement is improved by a factor of 1.6 in the above configuration. This improvement is primarily attributed to high edge temperature due to the reduction of anomalous transport. The inward shifted configuration contributes to the confinement improvement in the collision-less regime due to the neoclassical effect.

3. The absolute parameters of plasmas achieved in LHD experiments have been extended up to $T_e(0) \sim 4.4$ keV, $T_i(0) \sim 3.3$ keV, $n_e \sim 10^{20}$ m^{-3} and $\tau_E \sim 0.3$ s in maximum values. The plasma stored energy reached 0.88 MJ in a plasma of volume 30 m^3 with the heating instruments 1 MW of ECH, 4.2 MW of NBI, and 1.3 MW of ICRF. These parameters are translated to non-dimensional parameters like collisionality $\nu_e^* \sim \nu_i^* \sim 0.03 - 5$, normalized gyro radius $\rho^* \sim 1 - 5 \times 10^{-3}$, and $\beta \sim 2.4$ %.

4. The transition of the radial electric field from ion root to electron root is observed for the first time in the neutral beam heated plasmas, where there are no non-thermal electrons. The radial electric field observed was qualitatively explained by the neoclassical theory.

5. The fact that ICRF heating is effective to heat plasmas as well as tangential NBI heating indicates that energetic particles are well confined in LHD, in particular, in case of the inward shifted magnetic axis configuration.

6. Using multi-pellet injection, the density is raised up to $>10^{20}$ m^{-3} which exceeds the empirical scaling of the density limit by a factor of 2. The successful operation of higher dense plasmas comes from the benefit of scale of LHD plasmas as it has a size which is much

larger than the distance of neutral particle penetration and the core plasma is isolated from the radiation zone which is mainly localized to the outer edge region.

7. As for long pulse or steady state operation, LHD experiments demonstrated 80 s operation of 2 keV plasmas using NBI alone or ICRF. The pulse length is limited by the heating instruments capability and not by plasma behavior. The breathing oscillation is suppressed by reducing metallic impurity penetration using carbon tiles at the divertor plate. The operation time is much longer than the magnetic diffusion L/R time (around 3 s).

Acknowledgments

The authors would like to thank the scientists and the technical staff at the National Institute for Fusion Science who made these experiments possible and especially the former director-general, Professor A. Iiyoshi.

References

[1] Iiyoshi, A., et al., Fusion Technol. **17** (1990) 169.
[2] Motojima, O., et al., in Plasma Physics and Controlled Nuclear Fusion Research 1990 (Proc. 13th Int. Conf. Washington, DC, 1990), Vol.**3**, IAEA, Vienna (1991) 513.
[3] Iiyoshi, A., et al., Nucl. Fusion **39** (1999) 1245.
[4] Fujiwara, M., et al., Nucl. Fusion **39** (1999) 1659.
[5] Kawahata, K., Tanaka, K., Ito, Y., Ejiri, A., Okajima, S., Rev. Sci. Instrum. **70** (1999) 707.
[6] Narihara, K., et al., Fusion Engineering and Design **34-35** (1997) 67.
[7] Sudo, S., et al., Nucl. Fusion **30** (1990) 11.
[8] Strouth, U., et al., Nucl. Fusion **36** (1996) 1063.
[9] Ohyabu, N., et al., Phys. Rev. Lett. **84** (2000) 103.
[10] Erckmann, V., et al., Phys. Rev. Lett. **70** (1993) 2086.
[11] Toi, K., et al., in Plasma Physics and Contrlled Nuclear Fusion Research, 1992 (Proc. 14th Int. Conf. Wurtzburg, 1992), Vol.**2**, IAEA, Vienna (1993) 461.
[12] Itoh, K., et al., Plasma Phys. Control. Fusion **36** (1994) 1501.
[13] Yamazaki, K. et al., 26th EPS Conference (Maastricht, 1999) P3.107.
[14] Yamazaki, K. and Amano, T., Nucl. Fusion **32** (1992) 633.
[15] Yamada, H., et al., Phys. Rev. Lett. **84** (2000) 1216.
[16] Kadmotsev, B.B., Sov. J. Plasma Phys. **1** (1975) 295.
[17] Fujisawa. A. et al., Phys. Rev. Lett. **82** (2000) 2669.
[18] Mutoh, T. et al., Plasma Phys. Control. Fusion **42** (2000) 265.
[19] Kumazawa, R. et al., to be published in J. Plasma Fusion Res., SERIES Vol.**3** (2000).
[20] Krasilnikov, A. et al., J. of Plasma and Fusion Research **75** (1999) 967.
[21] Kaneko, O., et al., Nucl. Fusion **39** (1999) 1087.
[22] Okamura, S., et al., Nucl. Fusion **35** (1995) 283.
[23] Wagner, F., et al., in Plasma Physics and Contrlled Nuclear Fusion Research, 1998 (Proc. 17th Int. Conf. Tokohama, 1998), Vol.**1**, IAEA, Vienna (1999) 115.
[24] Osakabe, M., et al., to be published in Rev. Sci. Instrum. (2001).
[25] Mercier, C., Nucl. Fusion (Suppl. Pt. 2) (1962) 801.
[26] Sakakibara, S., et al., IAEA-CN-77/EXP3/12, this conference.
[27] Noda, N., et al., J. Plasma Fusion Res. SERIES **1** (1998) 130.
[28] Fujiwara, M., et al., J. Fusion Energy **15** (1987) 7.
[29] Takeiri, Y., et al., J. Plasma Fusion Res. SERIES **1** (1998) 405.
[30] Kumazawa, R., et al., Proceeding of 18th Sympo. on Fusion Technology **1** (1996) 617.
[31] Fujiwara, M., et al., Plasma Phys. Control. Fusion **41** (1999) B157.
[32] Motojima, O., et al., Phys. Plasmas **6** (1999) 1843.
[33] Peterson, B. J. et al., to be published in J. Plasma Fusion Res., SERIES Vol.**3** (2000).